

---

# Beyond position: how rotary embeddings shape representations and memory in autoregressive transformers

---

Valeria Ruscio

Fabrizio Silvestri

Sapienza University of Rome

ruscio@diag.uniroma1.it, fabrizio.silvestri@diag.uniroma1.it

## Abstract

Rotary Positional Embeddings (RoPE) enhance positional encoding in Transformer models, yet their full impact on model dynamics remains underexplored. This paper studies how RoPE introduces position-dependent rotations, causing phase shifts in token embeddings that influence higher-frequency components within the model’s internal representations. Through spectral analysis, we demonstrate that RoPE’s rotation matrices induce oscillatory behaviors in embeddings, affecting information retention across layers and shaping temporal modeling capabilities. We show that activation functions in feed-forward networks interact with RoPE-modulated embeddings to generate harmonics, leading to constructive or destructive interference based on phase alignment. Our findings reveal that phase alignment amplifies activations and sharpens attention, while misalignment weakens activations and disrupts focus on positional patterns. This study underscores the importance of frequency components as intrinsic elements of model behavior, offering new insights beyond traditional analyses.

are inherently permutation-invariant, incorporating positional information is crucial for the model to understand the sequential nature of language. Early methods used fixed sinusoidal encodings, while newer strategies, like Rotary Positional Embeddings (RoPE)[Su et al., 2024], apply rotation matrices directly to the token embeddings, integrating positional information through position-dependent rotations. These rotations introduce phase shifts in the embeddings’ vector components, effectively encoding each token’s position within the sequence.

Despite RoPE’s effectiveness, its impact on the internal dynamics of Transformer models—particularly its interaction with non-linear components like feed-forward neural networks (FFNs) and self-attention—remains underexplored. Understanding this interaction is essential for comprehending how Transformers process and retain sequential information, essential for tasks requiring nuanced temporal modeling. Our work studies three main aspects: the spectral properties of RoPE, its interactions with non-linear activation functions, and the emergence of constructive and destructive interference patterns due to phase alignment.

Our main contributions are: 1) Providing a detailed analysis of RoPE’s impact on internal model behavior and positional dependency modeling. 2) Studying how non-linearities in Transformers interact with RoPE to produce complex frequency patterns.

## 1 Introduction

Central to the Transformer architecture [Vaswani, 2017] is the self-attention mechanism, which allows the model to weight the influence of different parts of the input sequence when generating representations. However, because transformers

## 2 Related Works

The Transformer architecture introduced by [Vaswani, 2017] revolutionized sequence modeling using self-attention mechanisms, making recurrent or structures not necessary anymore. To provide the model with information about the token position in the sequence, the original Transformer used sinusoidal positional encodings added to the input embeddings. [Shaw et al., 2018] proposed relative positional encodings, integrating relative position information into self-attention to better generalize across varying se-

quence lengths. Dai et al. [Dai et al., 2018] extended this with Transformer-XL, enhancing the capture of long-term dependencies. [Huang et al., 2018] introduced the Music Transformer, which leverages relative positional encoding to model long-term structure in music generation tasks.

[Su et al., 2024] introduced Rotary Position Embedding (RoPE), applying rotation matrices to embeddings to introduce relative positional dependence through phase shifts, preserving inner product structures and enabling generalization to longer sequences.

Nonlinear systems, such as feedforward neural networks with activation functions like ReLU or GeLU, can generate higher-order harmonics and exhibit frequency mixing as studied by [Selesnick and Burrus, 1998]. Constructive and destructive interference are fundamental concepts in signal processing [Oppenheim, 1999], describing how overlapping waves can amplify or attenuate signals based on their phase alignment. By applying principles from signal processing, researchers have begun to analyze how frequency components and phase relationships affect neural network behavior. [Chi et al., 2020] investigated how convolutional neural networks process frequency information, highlighting the importance of understanding the spectral characteristics of activations. [Takahashi et al., 2018] explored adaptive modulation in neural networks, drawing parallels between neural activations and signal modulation techniques.

### 3 Methodology

Our study combines theoretical analysis with empirical experiments to explore how Rotary Positional Embeddings (RoPE) influence Transformer models. We conducted experiments using autoregressive Transformer models that implement Rotary Positional Embeddings (RoPE) for consistent positional encoding, specifically LLaMA 2, LLaMA 3 and LLaMA 3.1 [Touvron et al., 2023]. The primary results presented in the main paper are performed using LLaMA 3, with full experimental details and additional results provided in the appendix. Our study comprises two types of experiments aimed at understanding how phase shifts introduced by RoPE affect the models’ internal dynamics:

a) Phase Shift Simulations on Real Embeddings: In the first set of experiments, we investigated the impact of manual phase shifts on the attention mechanism by applying rotational transformations to the embeddings extracted from the models. We used 1,000 text samples, each containing 200 tokens, sourced from The BookCorpus [Zhu, 2015]. For each text sample, we

passed the input through the model to obtain the token embeddings before the application of positional encodings. After we manually applied rotation matrices to these embeddings to simulate phase shifts, the embeddings were then fed back into the model to study how the simulated phase shifts influenced the attention scores. This experiment aimed to understand the sensitivity of the model’s attention mechanism to phase differences introduced by RoPE.

b) Synthetic Sequence on FFN Activations: The second set of experiments focused on studying the effects of phase alignment and misalignment on the activations within the FFN of the models. We generated synthetic sequences to isolate the impact of input structure on phase interactions without altering the embedding rotations. These sequences consisted of repeated instances of the same token, since the tokens are identical, their embeddings (prior to positional encoding) are the same, promoting phase alignment after RoPE is applied, and sequences constructed by alternating between different tokens, resulting in varying embeddings and promoting phase misalignment. Each type comprised 250. We computed metrics such as variance, kurtosis, entropy, and the number of activation peaks to quantify differences in activation patterns between aligned and misaligned inputs.

Experiments were performed on Google Colab Pro with NVIDIA A100 GPU, using the Hugging Face Transformers library.

### 4 Spectral Properties

RoPE applies a rotation to the embedding vectors, parametrized by a frequency  $\theta_k$  for each dimension. For a position  $p$ , the embedding  $e(p)$  is rotated as:

$$e(p) = e(p) \cos(\theta_k p) + e^\perp(p) \sin(\theta_k p) \quad (1)$$

where  $e^\perp(p)$  is the orthogonal component of  $e(p)$ .

The spectral properties of the rotation matrices introduced by RoPE can be analyzed by considering the eigenvalues of these matrices. The eigenvalues of the rotation matrices represent the frequencies at which the embeddings are modulated due to the positional encoding. By computing these eigenvalues, we can understand how RoPE introduces phase shifts that vary with position, effectively encoding positional information into the embeddings.

Since these are rotation matrices, the eigenvalues lie on the unit circle in the complex plane, meaning that the rotation preserves the norm of the embeddings but alters their phase. Specifically, the rotation induces oscillatory behavior in the embedding space, which can be decomposed into frequency components.

#### 4.1 Eigenvalue and Spectral Analysis of RoPE

To deepen our understanding of how RoPE affects the embeddings’ behavior in Transformers, we examine the eigenvalues of the rotation matrices  $R_k(p)$  used in the positional encoding. While rotation matrices are known to have eigenvalues on the unit circle, analyzing them in the context of RoPE reveals important implications for the model’s temporal dynamics and memory retention capabilities.

Consider the 2D rotation matrix for dimension  $k$ :

$$R_k(p) = \begin{pmatrix} \cos(\phi_k) & -\sin(\phi_k) \\ \sin(\phi_k) & \cos(\phi_k) \end{pmatrix} \quad (2)$$

where  $\phi_k = \theta_k(p)$ .

The eigenvalues  $\lambda$  of  $R_k(p)$  satisfy:

$$\lambda = \cos \phi_k \pm i \sin \phi_k = e^{\pm i \phi_k} \quad (3)$$

These eigenvalues lie on the unit circle in the complex plane, with magnitude  $|\lambda| = 1$  and phase  $\phi_k = \theta_k(p)$ . This result illustrates that the rotation induced by RoPE causes the embeddings to oscillate with a frequency determined by  $\theta_k$ , and the phase changes linearly with position  $p$ .

This analysis shows how the choice of  $\theta_k$  affects the model’s sensitivity to positional changes. By understanding the eigenvalues, we can infer how RoPE modulates the embeddings to prioritize either long-term dependencies (slow phase changes) or short-term interactions (rapid phase changes), thereby impacting the model’s temporal dynamics and memory retention.

**Implications for temporal dynamics** as the sequence progresses, the embeddings undergo continuous rotations in their respective 2D subspaces. The linear change in phase with respect to position  $p$  means that embeddings at different positions have different phases, leading to oscillatory behavior. This directly impacts how the model processes sequential information, as the phase differences influence the dot-product attention calculations, leading to constructive or destructive interference patterns.

**Implications for Memory Retention and Temporal Processing** the frequency  $\theta_k$  determines the rate of phase change. Smaller values of  $\theta_k$  result in slower phase changes, meaning that embeddings retain more similarity over longer positional distances. This corresponds to longer memory retention in the model. Conversely, larger  $\theta_k$  values lead to faster phase changes, focusing the model’s attention on short-term dependencies. By selecting appropriate values for  $\theta_k$ , we can control the timescale over which the model retains information, effectively tuning the Transformer’s temporal processing capabilities. For example, in language modeling tasks involving long texts, setting

smaller  $\theta_k$  values allows the model to retain and integrate information from earlier parts of the text, enhancing its ability to understand overarching themes and plot developments. On the other hand, in real-time translation systems where recent words are more relevant, larger  $\theta_k$  values enable the model to quickly adapt to new inputs, improving translation accuracy for rapidly changing contexts.

## 5 Memory Dynamics

In Transformer models, RoPE modifies the incorporation of positional information by applying a rotation matrix  $R(p)$  to the queries and keys at each position  $p$ :

$$Q'(p) = R(p)Q(p), K'(p) = R(p)K(p) \quad (4)$$

The attention score between positions  $p$  and  $q$  becomes:

$$S(p, q) = \frac{Q'(p) \cdot K'(q)}{\sqrt{d_k}} = \frac{Q(p)^\top R(p)^\top R(q)K(q)}{\sqrt{d_k}} \quad (5)$$

Using the property that the transpose of a rotation matrix equals its inverse,  $R_k(p)^\top = R_k(p)^{-1}$ , and that  $R_k(p)^{-1}R(q) = R(q - p)$ , we simplify the attention score to:

$$S(p, q) = \frac{Q(p)^\top R(q - p)K(q)}{\sqrt{d_k}} \quad (6)$$

This expression shows that the attention score depends solely on the relative position  $\Delta p = q - p$ . The rotation  $R\Delta p$  introduces a phase shift affecting the alignment between  $Q(p)$  and  $K(q)$ . As  $|\Delta p|$  increases, the phase difference grows, potentially reducing the dot product due to misalignment. This leads to a natural decay of attention scores with increasing positional distance, effectively incorporating relative positional information into the model.

### 5.1 Relationship between $\theta_k$ and similarity

The relationship between the positional difference  $(p - q)$  and the frequency  $\theta_k$  plays a key role in the similarity between embeddings. When  $(p - q)\theta_k \approx \pi$ , the cosine of this value is close to -1, which can lead to interesting behaviors in how tokens at positions  $p$  and  $q$  are compared: i) Close Tokens, ii) Decay of Similarity and iii) Sign Flips and Oscillations.

When tokens are *close in position*,  $(p - q)\theta_k$  is small, and  $\cos(p - q)\theta_k$  is close to 1. This results in a high similarity between their embeddings, as expected. As  $(p - q)\theta_k$  increases, the cosine value decreases, reaching zero at  $(p - q)\theta_k = \frac{\pi}{2}$ . This implies a *decay in similarity* between tokens as their positional distance

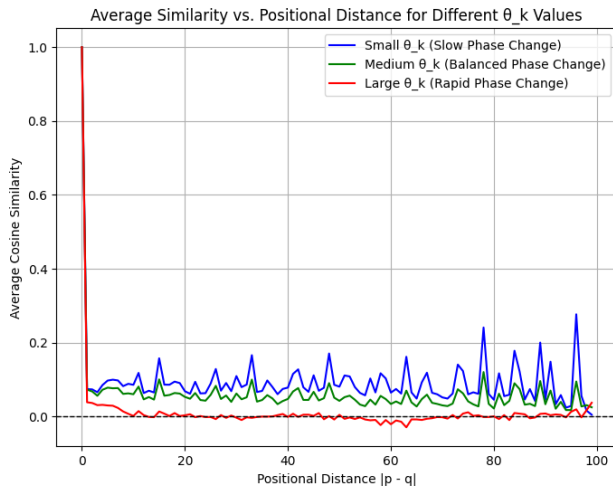


Figure 1: This plot shows how the cosine similarity between token embeddings decays with increasing positional distance, depending on the frequency parameter  $\theta_k$ .

grows. Once  $(p - q)\theta_k$  surpasses  $\frac{\pi}{2}$ , the cosine becomes negative. This leads to a situation where tokens that should be similar exhibit *negative similarity*, meaning their embeddings no longer align as intended. For example, an identical query might match a random key better than an identical key due to the cosine’s sign flip. This happens because if  $x_p^k \cdot x_q^k$  is positive (like when the embeddings are similar), but  $\cos((p - q)\theta_k)$  is negative, the similarity becomes negative. For a random key, the inner product  $x_p^k \cdot x_q^k$  is likely to be around 0, so the similarity would not be negative, making it appear as a better match than an identical key.

When  $(p - q)\theta_k \geq \pi$ , the cosine starts to increase again, which contradicts the idea of continuous decay<sup>1</sup>. The solution is bounding  $(p - q)\theta_k$  to ensure that it stays within a range where the cosine function behaves in a decaying way.

Figure 1 shows how the average cosine similarity changes when the positional distance for Various  $\theta_k$  values changes. The plot shows that embeddings with smaller  $\theta_k$  values maintain higher similarity over longer distances compared to those with larger  $\theta_k$  values, where small  $\theta_k = 0.01$ , medium  $\theta_k = 1$  and large  $\theta_k = 100$ .

## 5.2 Constructing the Memory Function

To analyze how RoPE influences the model’s ability to retain information over time, we consider the memory function  $M(n)$ , representing the cumulative effect of past inputs at lag  $n$ . Since RoPE introduces cosine

<sup>1</sup>This behaviour is due to cosine being an oscillatory function.

modulations into the attention mechanism, the memory function can be approximated as:

$$M(n) = \sum_{k=1}^K \alpha_k \cos(\theta_k n) \quad (7)$$

Here,  $\theta_k$  are the frequency components introduced by RoPE, and  $\alpha_k$  are weighting factors representing the contribution of each frequency component. The attention score between positions  $t$  and  $t - n$  is modulated by  $\cos(\theta_k n)$ , indicating that the influence of position  $t - n$  on position  $t$  oscillates and decays based on  $\theta_k$ .

This formulation resembles a Fourier series, where the memory function  $M(n)$  captures the cumulative effect of past inputs as a superposition of oscillatory components. The frequencies  $\theta_k$  and weights  $\alpha_k$  determine which temporal frequencies are emphasized or attenuated as information propagates through the network. If  $\alpha_k$  decreases for higher frequencies, the memory of distant past inputs decays more rapidly. The weights  $\alpha_k$  can be influenced by both the attention mechanism and the transformer’s inherent frequency response, potentially evolving across layers as the model dynamically adjusts its emphasis on different frequency components during processing.

Viewing the attention mechanism as performing temporal filtering, we formally derive the memory function using Fourier analysis. Suppose the input sequence  $x_t$  is decomposed into its frequency components:

$$x_t = \sum_k A_k e^{i\theta_k t} \quad (8)$$

Here,  $A_k$  are the Fourier coefficients, and  $\theta_k$  are the corresponding frequencies. The attention mechanism modulates these components by  $\cos(\theta_k n)$ :

$$\text{Attention}(x_t, x_{t-n}) \sim A_k \cos(\theta_k n) \quad (9)$$

The memory function then becomes:

$$M(n) = \sum_k |A_k|^2 \cos(\theta_k n) \quad (10)$$

This represents the cumulative influence of past inputs, modulated by the frequency components  $\theta_k$  introduced by RoPE. The presence of cosine terms implies that the memory function oscillates over time, with periods and amplitudes determined by  $\theta_k$  and  $\alpha_k$ . Depending on the distribution of  $\theta_k$ , the model may retain or attenuate certain temporal frequencies as information flows through the layers.

## 6 interactions with attention mechanism

In Transformer models, the attention mechanism selectively amplifies or suppresses different parts of the sequence based on learned attention weights, allowing the model to focus on relevant information. When combined with Rotary Position Embedding (RoPE), the interplay between phase shifts and nonlinearity leads to complex interactions where certain frequency components are enhanced or suppressed.

RoPE introduces phase shifts to the embeddings by applying a rotation that depends on the token’s position. Specifically, for each pair of embedding dimensions  $(2k, 2k+1)$ , the embedding is rotated by an angle proportional to the position index  $p$ :

$$q_p^{(2k)} = q^{(2k)} \cos(\theta_k p) - q^{(2k+1)} \sin(\theta_k p) \quad (11)$$

$$q_p^{(2k+1)} = q^{(2k)} \sin(\theta_k p) + q^{(2k+1)} \cos(\theta_k p) \quad (12)$$

and similarly for the key vectors  $k_q$ :

$$k_q^{(2k)} = k^{(2k)} \cos(\theta_k q) - k^{(2k+1)} \sin(\theta_k q) \quad (13)$$

$$k_q^{(2k+1)} = k^{(2k)} \sin(\theta_k q) + k^{(2k+1)} \cos(\theta_k q) \quad (14)$$

where  $q^{2k}$ ,  $q^{2k+1}$ ,  $k^{2k}$  and  $k^{2k+1}$  are components of the original query and key vectors, and  $\theta_k$  is the frequency parameter associated with the  $k$ -th dimension.

This means that the attention mechanism becomes sensitive not just to the content of the tokens but also to their relative positions. By encoding positional differences into the phase of embeddings, RoPE allows the model to capture patterns that depend on the distance between tokens, such as syntax structures or rhythmic patterns in text.

The attention score between positions  $p$  and  $q$  is computed as:

$$s_{pq} = \frac{\mathbf{q}_p^\top \mathbf{k}_q}{\sqrt{d_k}} \quad (15)$$

Substituting the rotated query and key vectors, and applying the rotation identities, we find that the dot product depends on the relative position  $\Delta p = q - p$ :

$$\mathbf{q}_p^\top \mathbf{k}_q = \sum_k k \left[ q^{(2k)} k^{(2k)} + q^{(2k+1)} k^{(2k+1)} \right] \cos(\theta_k \Delta p) \quad (16)$$

This shows that the attention score is modulated by a cosine function of the relative position, introducing an oscillatory behavior:

$$s_{pq} = \frac{1}{\sqrt{d_k}} \sum_k \left( q^{[k]} \cdot k^{[k]} \right) \cos(\theta_k (q - p)) \quad (17)$$

where  $q^{[k]} \cdot k^{[k]} = q^{2k} k^{2k} + q^{2k+1} k^{2k+1}$ . This expression shows that the dot product between the query and

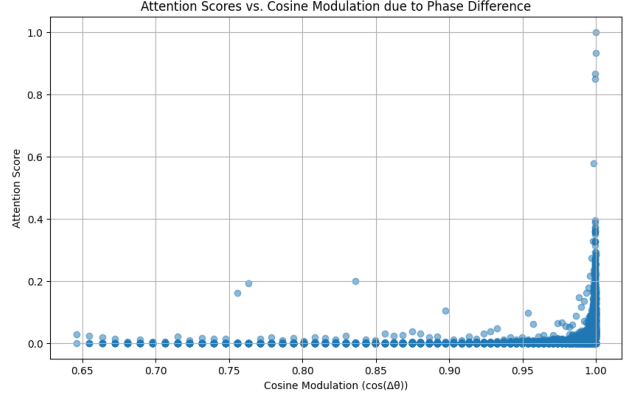


Figure 2: This scatter plot correlates attention scores with the cosine modulation term  $\cos(\Delta\theta)$ , where  $\Delta\theta = \theta_k(p - q)$  represents the phase difference.

key vectors is modulated by a cosine function of the relative position:

$$\mathbf{q}_p^\top \mathbf{k}_q \propto \cos(\theta_k(p - q)) \quad (18)$$

The rotational modulation of the embeddings by RoPE creates a form of frequency-based filtering, where certain phase differences lead to constructive interference (higher attention weights), while others lead to destructive interference (lower attention weights). This results in an oscillatory behavior in the attention scores, effectively modulating how different positions interact based on their relative distances and the frequency parameters  $\theta_k$ .

To investigate how phase differences introduced by RoPE affect the attention mechanism, we plotted the attention scores against the cosine of the phase difference ( $\cos \Delta\theta$ ) between token embeddings in Figure 2. The plot reveals a pronounced peak at  $(\cos \Delta\theta) = 1$ , corresponding to a phase difference of zero. This indicates that the model assigns the highest attention when there is no phase shift between tokens. As  $(\cos \Delta\theta)$  decreases, the attention scores decline sharply, showing the model’s sensitivity to even minor phase differences. This behavior suggests that phase alignment plays a critical role in the attention mechanism, with misaligned phases leading to diminished attention weights. Figure 3 illustrates the relationship between attention scores and positional difference  $(p - q)$ . The attention scores are highest when the positional difference is zero and decrease rapidly as the absolute value of  $(p - q)$  increases. This pattern indicates that the model predominantly focuses on tokens that are close to each other in the sequence. The rapid decline in attention with increasing positional distance suggests that RoPE effectively encodes positional information, causing the model to prioritize local context.

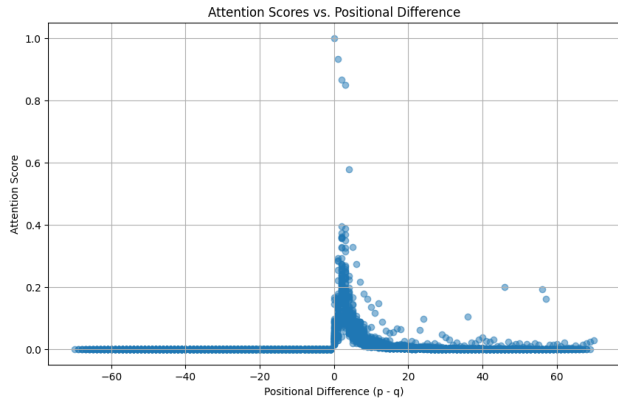


Figure 3: This scatter plot captures the attention scores between tokens at different positional distances ( $p - q$ ).

In practice, this would be very useful in time-series prediction tasks, since this property enables the model to focus on periodic patterns inherent in the data, such as daily or seasonal cycles. By adjusting  $\theta_k$ , we can tune the model to be more sensitive to specific frequencies, improving its ability to forecast future values based on historical periodic trends.

## 7 interactions with the Sftomax

The attention weights are computed using the softmax function:

$$\alpha_{pq} = \frac{\exp(s_{pq})}{\sum_j \exp(s_{pj})} \quad (19)$$

The softmax function is highly sensitive to variations in the attention scores  $s_{pq}$ . The oscillatory terms  $\cos(\theta_k(p - q))$  introduced by RoPE can lead to constructive or destructive interference, depending on the relative positions and frequency parameters. Small changes in  $s_{pq}$  can cause significant differences in the attention weights  $\alpha_{pq}$ , amplifying or attenuating the contributions from different positions.

To analyze how the nonlinearity of the softmax function affects the frequency components, we can consider a Taylor series expansion of the softmax function around the mean  $\bar{s}_p$ :

$$\text{softmax}(s_{pq}) \approx \frac{1}{N} + \frac{s_{pq} - \bar{s}_p}{N} + \frac{(s_{pq} - \bar{s}_p)^2}{2N} + \dots \quad (20)$$

where  $N$  is the number of positions in the sequence, and  $\bar{s}_p$  is the mean of  $s_{pq}$  over  $q$ .

By substituting the phase-dependent dot product into the expansion, we can see how the nonlinear softmax function introduces higher-order terms that influence the frequency components:

1) **The first-order term**  $\frac{s_{pq} - \bar{s}_p}{N}$ , captures the linear

relationship between the input and the output, preserving the original frequencies introduced by RoPE.

2) **The second-order term**  $\frac{(s_{pq} - \bar{s}_p)^2}{2N}$ , introduces nonlinearity by squaring the input. This term can generate new frequency components that are harmonics of the original frequencies, effectively doubling frequencies or creating combinations.

3) **Subsequent higher-order terms** in the expansion can introduce even more complex frequency interactions, including frequency mixing and the creation of new frequency components not present in the original signal.

These higher-order effects can be significant when the input (for example, the modulated dot product) has strong frequency components due to RoPE. The nonlinearity of the softmax function can amplify or attenuate certain frequencies, depending on the phase and amplitude of the input signal.

By expanding the softmax function, we observe that the RoPE-induced frequencies don't simply pass through the attention mechanism unaltered. Instead, they interact with the softmax's nonlinearity, which can enhance or suppress specific frequency components. The softmax function can be thought of as applying a nonlinear transformation that emphasizes the most significant attention scores (high-frequency components resulting from constructive interference) while diminishing less important ones (frequencies leading to destructive interference). This selective enhancement resembles the effect of a resonance filter that amplifies certain frequencies, shaping the model's sensitivity to specific positional relationships.

## 8 interactions with the FFN

After the attention mechanism, Transformers typically apply a feedforward neural network (FFN), introducing additional nonlinearity. The FFN can be represented as:

$$z = W_2 \cdot \sigma(W_1 x + b_1) + b_2 \quad (21)$$

where  $x$  is the input (the output of the attention mechanism, already RoPE-modulated),  $W_1$  and  $W_2$  are weight matrices,  $b_1$  and  $b_2$  are bias terms, and  $\sigma$  is a non-linear activation function (ReLU or GeLU).

The non-linear activation function  $\sigma$  introduces further nonlinearity by transforming the input in a non-linear fashion. This nonlinearity interacts with the frequency components of the input in several ways: i) **Harmonic Generation**, where non-linearities can introduce higher-order harmonics, adding new frequency components at integer multiples of the original frequencies. ii) **Waveform Distortion**, where the activation function can distort the waveform of the input signal, altering the amplitude and phase of the

frequency components. iii) **Phase Shifts**, where the linear transformations before and after the activation function can introduce phase shifts, affecting how different frequency components combine in the network.

### 8.1 Phase Modulation in the FFN with RoPE

Let  $x(p)$  represent the RoPE-modulated output of the attention head for the token at position  $p$ :

$$x(p) = R(p) \cdot a(p) \quad (22)$$

where  $a(p)$  is the unmodulated attention output, and  $R(p)$  is the RoPE rotation matrix applied at position  $p$ . For a given dimension pair  $k, k+1$ , RoPE introduces phase shifts:

$$\begin{aligned} x_k(p) &= a_k(p) \cos(\theta_k p) + a_{k+1}(p) \sin(\theta_k p) \\ &= -a_k(p) \sin(\theta_k p) + a_{k+1}(p) \cos(\theta_k p) \end{aligned}$$

where  $a_k(p)$  and  $a_{k+1}(p)$  are components of  $a(p)$ , and  $\theta_k$  is the frequency parameter associated with the  $k$ -th dimension. For the  $k$ -th neuron, substituting the phase-shifted expressions for  $x_k(p)$  and  $x_{k+1}(p)$ , we get:

$$\begin{aligned} h_k(p) &= [w_{k1} \cos(\theta_k p) - w_{k2} \sin(\theta_k p)] a_k(p) \\ &\quad + [w_{k1} \sin(\theta_k p) + w_{k2} \cos(\theta_k p)] a_{k+1}(p) + b_{1k} \end{aligned}$$

The first linear layer in the FFN mixes the phase-shifted components of the attention output. The coefficients  $w_{k1}$  and  $w_{k2}$  are modulated by trigonometric functions of the token’s position  $p$ , which means that the contribution of the attention outputs  $a_k(p)$  and  $a_{k+1}(p)$  to the FFN activations depends on the positional phase shifts introduced by RoPE.

This has two major effects:

1) *Frequency Mixing*: The interaction between the weight matrix  $W_1$  and the RoPE-induced phase shifts leads to frequency mixing. Each dimension of the embedding oscillates with a frequency determined by  $\theta_k$ . The linear transformation effectively mixes these oscillating components, resulting in new frequency components in the activations of the FFN.

2) *Positional Sensitivity*: Since the weights  $W_1$  are combined with the trigonometric functions  $\cos(\theta_k p)$  and  $\sin(\theta_k p)$ , the linear transformation encodes positional sensitivity into the FFN’s activations. Tokens at different positions contribute differently to the activations depending on their phase alignment.

After the linear transformation, the output passes through a non-linear activation function, such as ReLU or GeLU:

$$z_k(p) = \sigma(h_k(p)) \quad (23)$$

Non-linear activations introduce higher-order harmonics when applied to oscillatory inputs like the RoPE-modulated activations  $h_k(p)$ . This phenomenon is well-known in signal processing, where non-linearities applied to sinusoidal signals generate new frequency components (harmonics) at integer multiples of the original frequencies.

Considering the ReLU activation:

$$z_k(p) = \text{ReLU}(h_k(p)) \quad (24)$$

For an oscillatory input  $h_k(p)$  containing components like  $\cos(\theta_k p)$  and  $\sin(\theta_k p)$ , ReLU clips the negative parts of the oscillation, resulting in higher-order harmonics. Specifically: i) The fundamental frequency  $\theta_k$  remains present in the output. ii) Higher harmonics such as  $2\theta_k$ ,  $3\theta_k$ , etc., are generated due to the non-linearity introduced by ReLU. Mathematically, this harmonic generation can be described using the Fourier series expansion of a half-wave rectified sinusoid. For example:

$$\text{ReLU}(\cos(\theta_k p)) = \frac{1}{\pi} + \frac{1}{2} \cos(\theta_k p) - \frac{1}{\pi} \sum_{n=1}^{\infty} \frac{\cos(2n\theta_k p)}{4n^2 - 1} \quad (25)$$

This expansion shows that higher-order harmonics are introduced into the signal.

These harmonics enable the FFN to capture multi-scale dependencies in the sequence. Since RoPE causes embeddings at different positions to oscillate with different phases, the non-linearity can lead to constructive or destructive interference, depending on phase alignment.

**Constructive Interference** occurs when the phase shifts of different components  $h_k(p)$  are aligned; the non-linearity amplifies the output, resulting in stronger FFN activations. Thus, certain positional configurations reinforce each other, leading to higher neuron activations.

**Destructive Interference** happens when the phases are misaligned; components can cancel each other out, leading to weaker activations or even zero activations. This allows the FFN to selectively suppress certain positional patterns that are not relevant for the current token.

This means that the model can selectively enhance or suppress connections between tokens based on their positional relationships. For example, in a sentence where a subject and verb are separated by several words, constructive interference can reinforce their grammatical connection despite the distance. Conversely, destructive interference can help the model ignore irrelevant or less important tokens, such as filler words, by reducing their impact on the attention mechanism.

Mathematically, this interference can be analyzed

using trigonometric identities. For example, when two phase-shifted components  $\cos(\theta_k p)$  and  $\cos(\theta_{k+1} p)$  combine:

$$\begin{aligned} \cos(\theta_k p) + \cos(\theta_{k+1} p) = \\ 2 \cos\left(\frac{\theta_k + \theta_{k+1}}{2} p\right) \cos\left(\frac{\theta_k - \theta_{k+1}}{2} p\right) \end{aligned}$$

The term  $\cos\left(\frac{\theta_k + \theta_{k+1}}{2} p\right)$  represents a new cosine oscillation with a frequency equal to the average of the two original frequencies, while  $\cos\left(\frac{\theta_k - \theta_{k+1}}{2} p\right)$  modulates the amplitude based on the frequency difference. When the difference  $\theta_k - \theta_{k+1}$  is small,  $\cos\left(\frac{\theta_k - \theta_{k+1}}{2} p\right)$  is close to 1, and the signals reinforce each other, creating a stronger combined wave. If the difference is large,  $\cos\left(\frac{\theta_k - \theta_{k+1}}{2} p\right)$  oscillates rapidly between  $-1$  and  $1$  as  $p$  changes, leading to alternating constructive and destructive interference over different positions.

In the FFN, this phenomenon allows certain positional configurations to reinforce one another, leading to stronger neuron activations where frequencies (or phases) align. Conversely, misaligned frequencies lead to weaker activations or suppression of certain signals. This behavior, caused by the interference of the phase-modulated signals, makes the FFN sensitive to positional information and helps it selectively amplify or dampen features depending on token position. This capability is particularly important for tasks involving multi-scale dependencies, such as language modeling, where capturing harmonics allows for better representation of positional information at different granularities.

### 8.1.1 Second Linear Layer: Projecting Higher-Level Features

After the non-linear activation, the output is passed through the second linear transformation:

$$\text{FFN}(x) = W_2 \cdot z(p) + b_2 \quad (26)$$

The second linear layer  $W_2$  maps the non-linear activations back to the original embedding space or to a space compatible with the subsequent layers, effectively projecting the higher-level features extracted by the FFN. Since the input  $z(p)$  contains both the original RoPE-induced frequencies and the higher-order harmonics generated by the non-linearity,  $W_2$  acts as a frequency-selective filter that determines which features are propagated forward.

Two major effects occur in the second linear layer: i) Frequency Selection, since  $W_2$  can emphasize certain frequency components (for example, fundamental frequencies or specific harmonics) while attenuating others. This allows the FFN to focus on temporal or positional dependencies most relevant to the

task. ii) Higher-Level Feature Representation, because the second linear layer combines frequency-modulated features into a higher-level representation that captures both content-based and position-based information, crucial for handling the sequential nature of data in autoregressive Transformers.

## 9 Analysis

Our study shows that the rotation matrices used in RoPE introduce specific phase components into the token embeddings, leading to oscillatory behaviors characterized by distinct frequencies. When these frequency-modulated embeddings interact with the non-linear activation functions in the feed-forward neural networks (FFNs), higher-order harmonics are generated due to the nonlinearities introducing new frequency components. This interaction results in patterns of constructive and destructive interference based on the phase alignment of the embeddings. Constructive interference amplifies neuron activations, enhancing the model’s attention to key positional patterns, while destructive interference diminishes activations, potentially weakening the model’s ability to capture certain dependencies.

Drawing an analogy to signal processing, RoPE functions similarly to frequency modulation (FM) by adjusting the phase of embeddings according to positional information, enriching the representation space and enabling the model to capture positional nuances. The attention mechanism and FFNs act as nonlinear filters that shape the frequency content of these modulated signals in a context-sensitive manner, emphasizing or attenuating specific components based on the model’s learned parameters. The generation of harmonics through these nonlinearities expands the signal’s frequency spectrum, allowing the Transformer to represent more complex patterns and efficiently capture long-range dependencies. These dynamics enhance the model’s ability to adjust its focus dynamically, responding to context and varying sequential dependencies inherent in the input data.

## 10 Conclusion

In summary, our analysis shows that frequencies are intertwined with the operation of Transformers utilizing RoPE. The introduction of phase components and their interaction with non-linear activations generate oscillatory behaviors and interference patterns that significantly impact how information is processed across the model’s layers. Understanding these frequency dynamics provides valuable perspective into the internal workings of language models, unfolding on how they encode and manipulate sequential data.



## References

- [Chi et al., 2020] Chi, L., Jiang, B., and Mu, Y. (2020). Fast fourier convolution. *Advances in Neural Information Processing Systems*, 33:4479–4488.
- [Dai et al., 2018] Dai, Z., Yang, Z., Yang, Y., Cohen, W. W., Carbonell, J., Le, Q. V., and Salakhutdinov, R. (2018). Transformer-xl: Language modeling with longer-term dependency.
- [Huang et al., 2018] Huang, C.-Z. A., Vaswani, A., Uszkoreit, J., Shazeer, N., Simon, I., Hawthorne, C., Dai, A. M., Hoffman, M. D., Dinculescu, M., and Eck, D. (2018). Music transformer. *arXiv preprint arXiv:1809.04281*.
- [Oppenheim, 1999] Oppenheim, A. V. (1999). *Discrete-time signal processing*. Pearson Education India.
- [Selesnick and Burrus, 1998] Selesnick, I. W. and Burrus, C. S. (1998). Generalized digital butterworth filter design. *IEEE Transactions on signal processing*, 46(6):1688–1694.
- [Shaw et al., 2018] Shaw, P., Uszkoreit, J., and Vaswani, A. (2018). Self-attention with relative position representations. *arXiv preprint arXiv:1803.02155*.
- [Su et al., 2024] Su, J., Ahmed, M., Lu, Y., Pan, S., Bo, W., and Liu, Y. (2024). Roformer: Enhanced transformer with rotary position embedding. *Neurocomputing*, 568:127063.
- [Takahashi et al., 2018] Takahashi, N., Agrawal, P., Goswami, N., and Mitsufuji, Y. (2018). Phasenet: Discretized phase modeling with deep neural networks for audio source separation. In *Interspeech*, pages 2713–2717.
- [Touvron et al., 2023] Touvron, H., Lavril, T., Izacard, G., Martinet, X., Lachaux, M.-A., Lacroix, T., Rozière, B., Goyal, N., Hambro, E., Azhar, F., et al. (2023). Llama: Open and efficient foundation language models. *arXiv preprint arXiv:2302.13971*.
- [Vaswani, 2017] Vaswani, A. (2017). Attention is all you need. *Advances in Neural Information Processing Systems*.
- [Zhu, 2015] Zhu, Y. (2015). Aligning books and movies: Towards story-like visual explanations by watching movies and reading books. *arXiv preprint arXiv:1506.06724*.

## Appendix

---

### 11 ADDITIONAL EXPERIMENTS

This set of experiments focuses on studying the effects of phase alignment and misalignment on the activations within the FFN of the models. We generated 250 synthetic sequences to isolate the impact of input structure on phase interactions without altering the embedding rotations. These sequences consisted of repeated instances of the same token to promote phase alignment, and sequences constructed by alternating between different tokens, resulting in varying embeddings and promoting phase misalignment.

Consider a repeated token  $t$ , before applying RoPE, the embedding  $E(t)$  is identical at each position. After applying RoPE, the embedding at position  $p$  becomes:  $E'(p) = R(p)E(t)$ . The phase shift between positions  $p$  and  $q$  is:

$$\Delta\varphi = \theta(p - q) \tag{27}$$

where  $\theta$  is the rotational frequency parameter. The consistent phase increments lead to predictable interference patterns when computing dot products in attention mechanisms or processing through FFNs. In sequences with alternating tokens  $t_1$  and  $t_2$ , the embeddings before RoPE are  $E(t_1)$  and  $E(t_2)$ . After applying RoPE:

$$E'_1(p) = R(p)E(t_1) \tag{28}$$

$$E'_2(p + 1) = R(p + 1)E(t_2) \tag{29}$$

The phase difference between embeddings is influenced not only by positional differences but also by the inherent differences in  $E(t_1)$  and  $E(t_2)$ . This results in more complex interactions and potential cancellation effects within the model’s computations.

#### 11.1 Llama 2

In Llama 2 there’s a noticeable difference between the mean activations of aligned and misaligned sequences. The aligned sequences often have mean activations close to zero, while the misaligned sequences show varying mean values, sometimes positive and sometimes negative.

As we can see in Table 1, the **standard deviation** (Std) of activations is consistently higher for misaligned sequences compared to aligned sequences. This suggests that misaligned sequences produce more variable activations, possibly due to the complexity introduced by alternating tokens.

The **KS statistics** are significant across all layers (p-values effectively zero), indicating that the distributions of activations for aligned and misaligned sequences are statistically different. In Table 2 we show that the **t-statistics** show both positive and negative values, reflecting the direction of mean differences.

The t-statistics switch signs across layers, implying that in some layers, aligned sequences have higher mean activations, while in others, misaligned sequences do, this alternating pattern suggests that the model’s response to alignment varies throughout the network.

**For the Aligned Sequences** the consistent phase shifts lead to constructive interference, resulting in more stable and consistent activations (lower standard deviations).

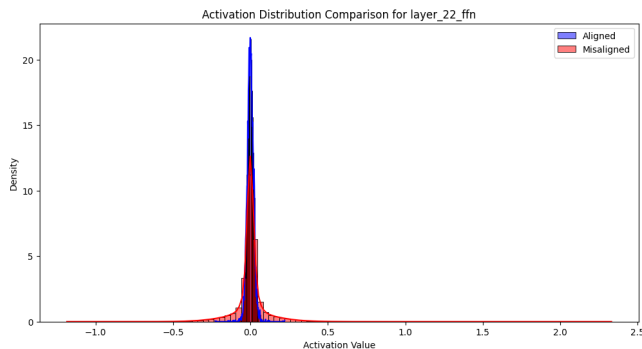


Figure 4: Activation distribution of Llama 2 at layer 22

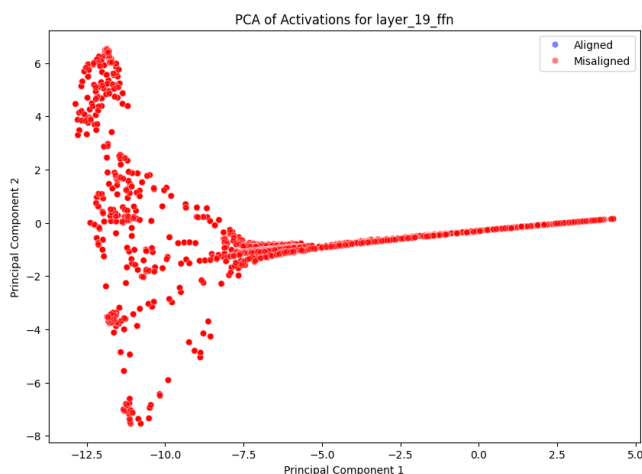


Figure 5: Scatter plot of the PCA of the FFN activations in Llama 2. In the plot we can only see red dots because they cover the blue ones representing the aligned sequences.

**Misaligned sequences** consistently exhibit higher standard deviations, indicating more dispersed activation values. This suggests that the model finds misaligned sequences more challenging to process, leading to less predictable activations

Despite significant differences in statistical measures, the high variability causes the distributions of activations to overlap, making it difficult to distinguish between aligned and misaligned sequences using linear methods like **PCA** as we show in Figure 2. Higher **variance** in aligned activations suggests that the model is actively processing and transforming aligned sequences with a wider range of activation values, as shown in Table 3. Misaligned sequences may result in less dynamic processing initially, possibly due to the model’s uncertainty or inability to effectively integrate misaligned positional information. The increase in variance for misaligned activations in deeper layers indicates that the model starts to generate more diverse activations when processing misaligned sequences. This could be due to the accumulation of errors or interference patterns introduced by misalignment, leading to unstable or erratic activations.

The higher **Kurtosis** in misaligned activations indicates that misaligned sequences produce activations with more extreme values, possibly due to destructive interference or the model’s difficulty in processing misaligned positional information. Certain layers exhibit dramatic differences in kurtosis between aligned and misaligned activations, highlighting layers that are particularly sensitive to positional misalignment.

The higher **entropy** in misaligned activations suggests that the model’s activations are more random when processing misaligned sequences, reflecting uncertainty or instability in the internal representations. And the increase in entropy for misaligned activations in deeper layers (as we can see in Table 4) may indicate that the model’s confusion accumulates as it processes misaligned positional information.

We also find an increased number of **peaks** in misaligned activations, and it may reflect the presence of interference patterns causing fluctuations in activations across sequence positions and that misaligned sequences lead

to less stable activation profiles.

**Layer-Specific Behaviors** certain layers (e.g., Layer 1, Layer 4, Layer 21) show particularly large differences in means and standard deviations. These layers may be more sensitive to positional information and the interference patterns caused by RoPE phase shifts.

The variation in t-statistics and standard deviations across layers indicates that the model integrates positional information differently at each layer. Early layers might capture immediate positional effects, while deeper layers might aggregate information over longer contexts.

The dramatic increase in kurtosis and entropy in misaligned activations in deeper layers suggests that the model’s capacity to handle misalignment diminishes as it progresses through the network.

**In conclusion** the data from Llama 2 reveals significant statistical differences between aligned and misaligned sequences in terms of mean activations, standard deviations, and distribution shapes across layers. However, the high variability, particularly in misaligned sequences, leads to overlapping activation distributions that challenge linear separation methods like PCA. As the model processes misaligned sequences through deeper layers, variance, kurtosis, and entropy often increase, indicating accumulating interference effects and the model’s internal representations become more erratic and less stable, reflecting the disruptive impact of positional misalignment. These findings suggest that: i) interference patterns matter, in fact, constructive and destructive interference due to RoPE phase shifts have a substantial impact on the model’s activations; ii) high within-class variability can mask the differences between classes, necessitating alternative analytical approaches.

### 11.2 Llama 3

As we can see from Table 5, the tests performed on Llama 3 show that the **mean activations** for both aligned and misaligned sequences are very close to zero across all layers. The differences between the means of aligned and misaligned sequences are minimal, often in the order of  $10^{-4}$  or  $10^{-3}$ . The **standard deviations** for both aligned and misaligned sequences are very similar within each layer. There is a gradual increase in standard deviation as we move to deeper layers, which is typical in deep neural networks due to the accumulation of variance.

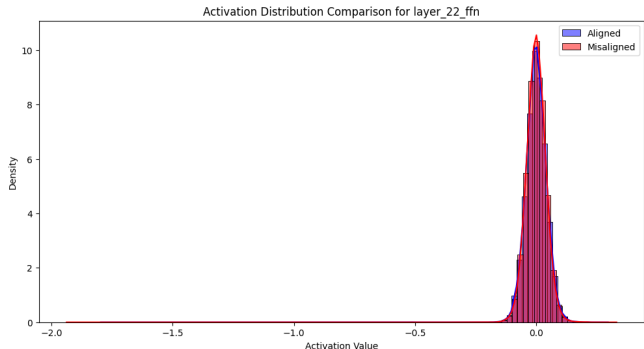


Figure 6: Activation distribution of Llama 3 at layer 22

The KS statistics are low across all layers, indicating that the distributions of activations for aligned and misaligned sequences are very similar. P-values are effectively zero due to the large sample size, but the low KS statistics suggest minimal differences in distributions, as we show in Table 6. The t-statistics show both positive and negative values, reflecting small differences in mean activations. However, the absolute values of the t-statistics are generally lower compared to Llama 2, except for some layers (e.g., Layer 10 with a t-statistic of -210.5745), indicating less pronounced mean differences. Despite smaller differences in statistical measures, **PCA** plots showed clear separation between aligned and misaligned sequences, and Figure 4 is an example of this phenomenon. This suggests that the variance relevant to sequence alignment is captured effectively in the principal components. In fact, the activations seem to have tighter distributions with less overlap between classes, and a small mean differences combined with low variability result in distinct clusters in PCA space. This suggests that Llama 3 seems to have **specialized neurons** that respond differently to aligned and misaligned sequences, capturing class differences effectively.

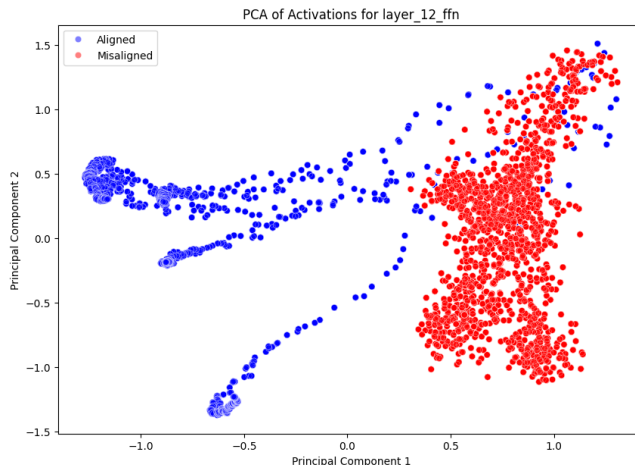


Figure 7: Scatter plot showing the PCA of the FFN activations for aligned and misaligned sequences.

In table 7 we can see the **variance** for both aligned and misaligned activations generally increases, which is expected as the model processes and transforms the input data. This pattern suggests that beyond the initial layer, the model might be compensating for the misalignment, or the impact of misalignment on variance diminishes as the data is processed deeper into the network.

Also the **kurtosis** values fluctuate, with some layers showing higher kurtosis for aligned activations and others for misaligned. For instance, in Layer 2, misaligned activations have a higher kurtosis (45.979829) than aligned activations (7.127898), suggesting that misalignment leads to more extreme activation values in certain layers. These fluctuations indicate that the impact of misalignment on the distribution of activations varies across layers, possibly due to the differing functions and sensitivities of each layer.

**The higher variance and kurtosis** in misaligned activations, especially in the initial layers, suggest that misalignment introduces more variability and extreme activation values. This could be due to interference patterns caused by misalignment, disrupting the model’s ability to process sequences coherently.

**Entropy** values for both aligned and misaligned activations are relatively similar, with minor differences. For example, in Layer 6, the entropy for aligned activations is 2.189469, and for misaligned activations, it is slightly higher at 2.260520, as shown in Table 8. These small differences suggest that misalignment may introduce slightly more randomness in certain layers, but the overall effect on entropy is not substantial. The entropy differences between aligned and misaligned activations are relatively minor in most layers, implying that the overall randomness in activation distributions is not drastically affected by misalignment. However, the slightly higher entropy in misaligned activations may reflect additional uncertainty introduced by misalignment.

**The misaligned** activations consistently exhibit a higher number of peaks than the aligned activations. For instance, in Layer 2, misaligned activations have 112 peaks, whereas aligned activations have 41. This pattern persists in many layers, indicating that misaligned sequences produce more complex activation patterns across sequence positions. The consistently higher number of activation peaks in misaligned activations indicates more erratic activation patterns across sequence positions. This suggests that misalignment leads to fluctuations in the activations as the model struggles to integrate positional information correctly.

**In some layers** the differences between aligned and misaligned activations are less pronounced. For example, in Layer 1, the variance and entropy are nearly identical for both, and the kurtosis values are extremely high for both aligned and misaligned activations. This could indicate that the model is somewhat robust to misalignment at this layer, or that both aligned and misaligned sequences result in similar activation patterns due to the specific computations performed.

**In conclusion** these results show that Llama 3 effectively distinguishes between aligned and misaligned sequences despite smaller differences in mean activations and standard deviations. The clear separation observed in PCA plots indicates that Llama 3 captures the variance related to sequence alignment along specific principal

components. This suggests that the model’s internal representations of positional information are both discriminative and efficiently organized, leading to tighter activation distributions with less overlap between the two types of sequences.

The findings also suggest that positional misalignment introduces interference patterns that affect the model’s processing, particularly in terms of increased variability, presence of extreme values, and more complex activation patterns. These effects are more pronounced in some layers than others, indicating that certain layers are more sensitive to positional misalignment. The increased variance and kurtosis in misaligned activations point to potential interference patterns disrupting the model’s processing, which could impact performance on tasks requiring precise positional information. The higher number of activation peaks in misaligned sequences suggests that the model’s activations are more erratic when positional information is misaligned, potentially leading to less stable representations. This could have implications for tasks where consistent internal representations are crucial.

### 11.3 Llama 3.1

As shown in Figure 5 and Table 9, for Llama 3.1 the mean activations for both aligned and misaligned sequences are close to zero across all layers. Differences between the means of aligned and misaligned sequences are small, often in the order of  $10^{-4}$  to  $10^{-3}$ .

The **standard deviations** are similar between aligned and misaligned sequences within each layer, but there is a slight increase in standard deviations in deeper layers, which is expected due to the accumulation of variance in deep networks. KS statistics are low across all layers, indicating minimal differences between the activation

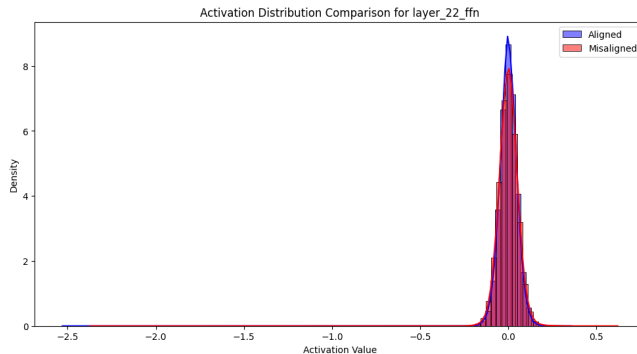


Figure 8: Activations distribution of Llama 3.1 at layer 22

distributions of aligned and misaligned sequences and P-values are effectively zero due to large sample sizes, but the low KS statistics suggest that the distributions are quite similar. The **t-statistics** vary in magnitude and sign across layers: in fact, some layers show high absolute t-statistics (for example in layer 3), indicating statistically significant mean differences, albeit small in absolute terms. The p-values are generally very low, indicating statistical significance, but this is influenced by the sample sizes, as shown in Table 10.

As for Llama 3, even if the differences in statistical measures are on the smaller side, **PCA** plots showed clear separation between aligned and misaligned sequences. This suggests that the variance relevant to sequence alignment is captured effectively in the principal components. In Llama 3.1 we find a slightly less clear separation though, like in Figure 6, where we can see that part of the dots representing the activations for aligned sequences are covered by the red dots. This still suggests that also Llama 3.1 seems to have **specialized neurons** that respond differently to aligned and misaligned sequences, capturing class differences effectively. The small differences in mean activations suggest that Llama 3.1 processes aligned and misaligned sequences similarly in terms of average activation levels. However, the increased standard deviations indicate that misaligned sequences may introduce more variability due to destructive interference from RoPE phase shifts. Changes in model architecture, training data, or regularization techniques between Llama 3 and Llama 3.1 could contribute to the observed differences.

In Table 11 we can see that as we progress through the layers, the **variance** for both aligned and misaligned activations generally increases, which is expected as the model processes and transforms the input data, leading to more complex representations. The variance is relatively similar between aligned and misaligned activations,

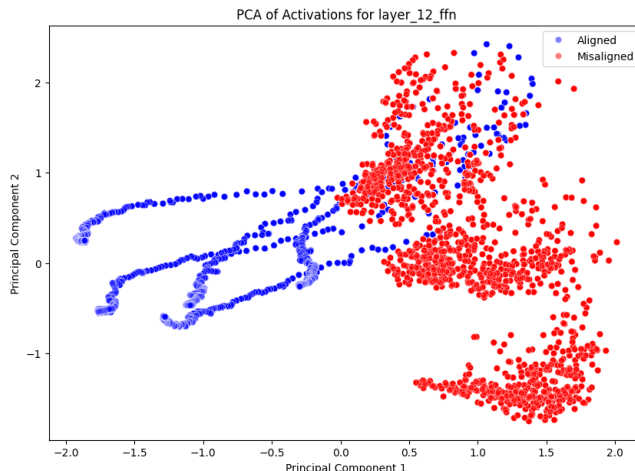


Figure 9: In the PCA plot we can only see red dots because they cover the blue ones representing the eligned sequences.

with minor fluctuations. In deeper layers (e.g., Layers 19-31), misaligned activations sometimes have slightly higher variance, which may indicate that the effects of misalignment accumulate over the layers, leading to increased variability in the activations.

In Layer 0, misaligned activations have a significantly higher **kurtosis** (375.936553) compared to aligned activations (38.748624). This substantial difference suggests that misaligned sequences produce activations with more extreme values, possibly due to interference patterns caused by positional misalignment. Throughout the layers, kurtosis values fluctuate, indicating that the impact of misalignment on the distribution of activations varies across layers, possibly due to the differing functions and sensitivities of each layer. Layers that show higher kurtosis in misaligned activations may be more sensitive to positional discrepancies.

As shown in Table 12, **Entropy** values increase through the layers and it shows minor differences between aligned and misaligned activations, this suggests that misalignment may introduce slight increases in randomness or uncertainty in the activations at certain layers, but the overall effect on entropy is not substantial.

Throughout the layers, misaligned activations consistently exhibit a **higher number of peaks** than aligned activations. This consistent pattern indicates that misaligned sequences produce more complex or erratic activation patterns across sequence positions, potentially due to the model’s difficulty in integrating positional information when misaligned.

**Misaligned activations** often show higher variance and kurtosis, especially in the initial layers. This indicates that positional misalignment introduces more variability and results in activations with more extreme values. These extreme values could be due to destructive interference patterns caused by misalignment, where the model’s expectations of positional information are disrupted, leading to irregular activation magnitudes.

The higher number of activation peaks in misaligned activations suggests that misalignment leads to more fluctuations in activation patterns across the sequence positions. This could be due to the model receiving conflicting positional cues, causing it to activate different neurons inconsistently across the sequence.

**Layer-Specific Behaviors** the model appears to rely heavily on positional information in the early layers to build coherent internal representations. Misalignment disrupts this process, leading to increased variability and erratic activation patterns. As the data progresses through the network, the model may compensate for misalignment to some extent, but the initial disruptions can have lasting effects.

Some layers show higher kurtosis or variance in aligned activations, indicating that the model’s processing of aligned sequences can also lead to extreme activation values, possibly due to amplification of certain features.

In the deeper layers, the differences in metrics between aligned and misaligned activations become more nuanced: while variance remains similar, kurtosis and the number of peaks often remain higher in misaligned activations, suggesting that the effects of misalignment persist but may be partially mitigated by the network’s depth.

**Misalignment** leads to increased variance and kurtosis, indicating that activations become more scattered and extreme. This can degrade the model’s ability to extract meaningful features from the input sequences. The higher number of activation peaks in misaligned activations suggests that the model’s internal representations are less stable, potentially affecting downstream tasks that rely on consistent feature extraction. So, identifying layers that are more sensitive to misalignment can help target interventions. For example, adjusting the positional encoding mechanism or adding regularization techniques in these layers might mitigate the negative effects.

**In conclusion** the analysis of Llama 3.1’s activations reveals that while the model still distinguishes between aligned and misaligned sequences, the separation is less pronounced than in Llama 3. Small differences in mean activations and slightly higher standard deviations suggest that Llama 3.1 exhibits increased variability in its activations, particularly for misaligned sequences. This increased within-class variance leads to more overlap in activation distributions and reduces the effectiveness of PCA in separating the classes. These findings indicate that Llama 3.1 may be less efficient at leveraging positional encoding to differentiate between sequence alignments compared to Llama 3. The reduced separation in PCA plots suggests that the variance associated with class differences is not as strongly captured in the principal components. It looks like Misaligned sequences often lead to increased variance and kurtosis in activations, indicating more variability and extreme values. Also, there is a consistent increase in the number of activation peaks for misaligned sequences across layers, suggesting more erratic activation patterns.

#### 11.4 Tables



Table 1: Means and Standard Deviations of Activations Llama 2

Layer	Aligned Mean	Aligned Std	Misaligned Mean	Misaligned Std
Layer 0	-0.0000	0.0310	0.0002	0.0302
Layer 1	0.0565	13.7587	0.0113	4.3314
Layer 2	-0.0005	0.0999	-0.0004	0.0785
Layer 3	0.0000	0.0106	-0.0001	0.0250
Layer 4	-0.0028	0.2404	-0.0010	0.1410
Layer 5	0.0003	0.0181	0.0004	0.0323
Layer 6	0.0002	0.0146	0.0002	0.0377
Layer 7	-0.0001	0.0152	-0.0001	0.0380
Layer 8	0.0002	0.0164	0.0003	0.0412
Layer 9	-0.0001	0.0178	-0.0001	0.0454
Layer 10	0.0000	0.0217	-0.0003	0.0520
Layer 11	0.0003	0.0247	0.0001	0.0542
Layer 12	0.0002	0.0181	0.0000	0.0583
Layer 13	-0.0002	0.0216	-0.0007	0.0668
Layer 14	0.0002	0.0199	-0.0003	0.0734
Layer 15	0.0000	0.0317	-0.0004	0.0898
Layer 16	0.0017	0.3057	0.0006	0.2275
Layer 17	-0.0005	0.0247	0.0001	0.0988
Layer 18	0.0002	0.0200	0.0006	0.0962
Layer 19	0.0029	0.2310	0.0021	0.1632
Layer 20	-0.0007	0.0258	-0.0006	0.0914
Layer 21	-0.0003	0.0251	-0.0014	0.0905
Layer 22	-0.0004	0.0215	-0.0002	0.0961
Layer 23	-0.0004	0.0288	0.0002	0.0851
Layer 24	-0.0003	0.0225	-0.0003	0.1058
Layer 25	-0.0010	0.0357	-0.0010	0.1160
Layer 26	-0.0007	0.0259	-0.0018	0.1260
Layer 27	-0.0012	0.0587	-0.0023	0.1634
Layer 28	-0.0006	0.0432	-0.0016	0.1678
Layer 29	0.0020	0.1829	-0.0015	0.2456
Layer 30	-0.0349	9.5605	-0.0107	2.2626
Layer 31	0.0058	0.7895	0.0208	2.7727

Table 2: Statistical Tests Results on Llama 2 FFN activations

Layer	KS Statistic	KS p-value	t-Statistic	t-test p-value
Layer 0	0.0378	0.0	-44.8944	0.0
Layer 1	0.2601	0.0	32.0735	$1.0334 \times 10^{-225}$
Layer 2	0.0603	0.0	-8.5045	$1.8242 \times 10^{-17}$
Layer 3	0.0793	0.0	49.8652	0.0
Layer 4	0.1608	0.0	-67.6719	0.0
Layer 5	0.0978	0.0	-19.9680	$1.0451 \times 10^{-88}$
Layer 6	0.1015	0.0	2.2374	$2.5260 \times 10^{-2}$
Layer 7	0.0991	0.0	4.1280	$3.6595 \times 10^{-5}$
Layer 8	0.0990	0.0	-13.0585	$5.6839 \times 10^{-39}$
Layer 9	0.0910	0.0	4.7302	$2.2434 \times 10^{-6}$
Layer 10	0.0952	0.0	67.2831	0.0
Layer 11	0.0843	0.0	21.1296	$4.2522 \times 10^{-99}$
Layer 12	0.1050	0.0	19.1474	$1.0177 \times 10^{-81}$
Layer 13	0.1129	0.0	81.6957	0.0
Layer 14	0.1188	0.0	59.6911	0.0
Layer 15	0.1069	0.0	49.1412	0.0
Layer 16	0.0633	0.0	28.7902	$2.8467 \times 10^{-182}$
Layer 17	0.1228	0.0	-62.8497	0.0
Layer 18	0.1410	0.0	-41.4314	0.0
Layer 19	0.0787	0.0	31.0820	$4.2218 \times 10^{-212}$
Layer 20	0.1169	0.0	-13.4339	$3.8257 \times 10^{-41}$
Layer 21	0.1255	0.0	113.2958	0.0
Layer 22	0.1472	0.0	-15.7370	$8.4295 \times 10^{-56}$
Layer 23	0.1346	0.0	-67.1515	0.0
Layer 24	0.1671	0.0	-5.2423	$1.5862 \times 10^{-7}$
Layer 25	0.1376	0.0	-2.9775	$2.9063 \times 10^{-3}$
Layer 26	0.1837	0.0	90.9769	0.0
Layer 27	0.1319	0.0	67.0804	0.0
Layer 28	0.1768	0.0	57.1779	0.0
Layer 29	0.0594	0.0	117.4058	0.0
Layer 30	0.0464	0.0	-25.2003	$3.9785 \times 10^{-140}$
Layer 31	0.1882	0.0	-53.1113	0.0

Table 3: FFN Activations Variance and Kurtosis Values per Layer for Lama 2

Layer	Aligned Variance	Misaligned Variance	Aligned Kurtosis	Misaligned Kurtosis
Layer 0	0.000958	0.000909	147.376870	450.293038
Layer 1	189.301910	18.760889	2517.226552	9584.869177
Layer 2	0.009974	0.006163	942.513140	1207.720646
Layer 3	0.000112	0.000626	12.324369	301.364062
Layer 4	0.057784	0.019875	251.488492	537.800603
Layer 5	0.000329	0.001046	469.139445	32.133494
Layer 6	0.000214	0.001422	149.209058	15.636808
Layer 7	0.000230	0.001446	55.386710	14.914418
Layer 8	0.000268	0.001696	168.355079	41.643733
Layer 9	0.000317	0.002059	131.712825	11.949710
Layer 10	0.000472	0.002705	70.363190	36.411350
Layer 11	0.000608	0.002938	125.090690	37.491922
Layer 12	0.000328	0.003399	33.755511	11.014107
Layer 13	0.000465	0.004461	101.965093	36.300238
Layer 14	0.000394	0.005394	31.122054	9.695558
Layer 15	0.001007	0.008062	40.867651	62.675431
Layer 16	0.093446	0.051771	69.587139	83.290888
Layer 17	0.000612	0.009752	21.746094	97.290267
Layer 18	0.000401	0.009262	21.032534	63.357352
Layer 19	0.053355	0.026626	65.022751	69.923168
Layer 20	0.000663	0.008347	6.739614	50.176895
Layer 21	0.000629	0.008196	5.125684	11.852076
Layer 22	0.000462	0.009230	9.428607	9.702882
Layer 23	0.000831	0.007249	10.111835	9.616285
Layer 24	0.000505	0.011194	7.011010	8.283153
Layer 25	0.001272	0.013451	8.439607	351.566518
Layer 26	0.000673	0.015878	4.999129	13.778022
Layer 27	0.003445	0.026703	7.704944	8.603530
Layer 28	0.001863	0.028152	9.563569	10.354717
Layer 29	0.033438	0.060331	153.936535	8.230512
Layer 30	91.402138	5.119313	2536.507203	17761.817783
Layer 31	0.623273	7.688102	84.248899	1111.958487

Table 4: Activations Entropy and Number of Peaks per Layer for Llama 2

Layer	Aligned Entropy	Misaligned Entropy	Aligned Peaks	Misaligned Peaks
Layer 0	2.286771	2.148640	89	127
Layer 1	0.036389	0.010554	78	40
Layer 2	1.239760	1.093074	76	65
Layer 3	2.839637	3.397158	81	84
Layer 4	1.765312	1.179644	57	62
Layer 5	1.978643	2.603812	72	90
Layer 6	2.397626	3.013041	73	80
Layer 7	2.528681	3.194545	87	80
Layer 8	2.296124	2.945954	71	96
Layer 9	2.285897	2.958959	81	93
Layer 10	2.430262	3.093451	82	91
Layer 11	2.285858	2.907948	73	65
Layer 12	2.538281	3.317049	80	86
Layer 13	2.302424	3.115713	79	82
Layer 14	2.578832	3.449447	77	92
Layer 15	2.596895	3.356084	87	89
Layer 16	2.291857	2.060505	77	82
Layer 17	2.786680	3.609248	71	94
Layer 18	2.823713	3.707424	80	78
Layer 19	2.307882	2.066757	63	75
Layer 20	3.022282	3.754197	72	82
Layer 21	3.135118	3.825276	78	74
Layer 22	2.925587	3.800145	71	96
Layer 23	2.883445	3.724280	77	94
Layer 24	3.023099	3.945461	72	97
Layer 25	2.989809	3.815957	62	95
Layer 26	3.144766	4.070633	75	93
Layer 27	3.031415	3.812775	53	76
Layer 28	3.051819	4.006574	83	89
Layer 29	2.023154	2.333842	77	87
Layer 30	3.022282	3.754197	72	82
Layer 31	2.240728	3.235996	88	69

Table 5: FFN Activations Variance and Kurtosis Values per Layer for Lama 3

Layer	Aligned Mean	Aligned Std	Misaligned Mean	Misaligned Std
Layer 0	0.0001	0.0145	0.0001	0.0226
Layer 1	-0.0002	0.4865	-0.0004	0.4864
Layer 2	-0.0005	0.0999	-0.0004	0.0785
Layer 3	0.0000	0.0106	-0.0001	0.0250
Layer 4	-0.0028	0.2404	-0.0010	0.1410
Layer 5	0.0003	0.0181	0.0004	0.0323
Layer 6	0.0002	0.0146	0.0002	0.0377
Layer 7	-0.0001	0.0152	-0.0001	0.0380
Layer 8	0.0002	0.0164	0.0003	0.0412
Layer 9	-0.0001	0.0178	-0.0001	0.0454
Layer 10	0.0000	0.0217	-0.0003	0.0520
Layer 11	0.0003	0.0247	0.0001	0.0542
Layer 12	0.0002	0.0181	0.0000	0.0583
Layer 13	-0.0002	0.0216	-0.0007	0.0668
Layer 14	0.0002	0.0199	-0.0003	0.0734
Layer 15	0.0000	0.0317	-0.0004	0.0898
Layer 16	0.0017	0.3057	0.0006	0.2275
Layer 17	-0.0005	0.0247	0.0001	0.0988
Layer 18	0.0002	0.0200	0.0006	0.0962
Layer 19	0.0029	0.2310	0.0021	0.1632
Layer 20	-0.0007	0.0258	-0.0006	0.0914
Layer 21	-0.0003	0.0251	-0.0014	0.0905
Layer 22	-0.0004	0.0215	-0.0002	0.0961
Layer 23	-0.0004	0.0288	0.0002	0.0851
Layer 24	-0.0003	0.0225	-0.0003	0.1058
Layer 25	-0.0010	0.0357	-0.0010	0.1160
Layer 26	-0.0007	0.0259	-0.0018	0.1260
Layer 27	-0.0012	0.0587	-0.0023	0.1634
Layer 28	-0.0006	0.0432	-0.0016	0.1678
Layer 29	0.0020	0.1829	-0.0015	0.2456
Layer 30	-0.0349	9.5605	-0.0107	2.2626
Layer 31	0.0058	0.7895	0.0208	2.7727

Table 6: Statistical Tests Results on Llama 3 FFN activations

Layer	KS Statistic	KS p-value	t-Statistic	t-test p-value
Layer 0	0.0378	0.0	-44.8944	0.0
Layer 1	0.2601	0.0	32.0735	$1.0334 \times 10^{-225}$
Layer 2	0.0603	0.0	-8.5045	$1.8242 \times 10^{-17}$
Layer 3	0.0793	0.0	49.8652	0.0
Layer 4	0.1608	0.0	-67.6719	0.0
Layer 5	0.0978	0.0	-19.9680	$1.0451 \times 10^{-88}$
Layer 6	0.1015	0.0	2.2374	$2.5260 \times 10^{-2}$
Layer 7	0.0991	0.0	4.1280	$3.6595 \times 10^{-5}$
Layer 8	0.0990	0.0	-13.0585	$5.6839 \times 10^{-39}$
Layer 9	0.0910	0.0	4.7302	$2.2434 \times 10^{-6}$
Layer 10	0.0952	0.0	67.2831	0.0
Layer 11	0.0843	0.0	21.1296	$4.2522 \times 10^{-99}$
Layer 12	0.1050	0.0	19.1474	$1.0177 \times 10^{-81}$
Layer 13	0.1129	0.0	81.6957	0.0
Layer 14	0.1188	0.0	59.6911	0.0
Layer 15	0.1069	0.0	49.1412	0.0
Layer 16	0.0633	0.0	28.7902	$2.8467 \times 10^{-182}$
Layer 17	0.1228	0.0	-62.8497	0.0
Layer 18	0.1410	0.0	-41.4314	0.0
Layer 19	0.0787	0.0	31.0820	$4.2218 \times 10^{-212}$
Layer 20	0.1169	0.0	-13.4339	$3.8257 \times 10^{-41}$
Layer 21	0.1255	0.0	113.2958	0.0
Layer 22	0.1472	0.0	-15.7370	$8.4295 \times 10^{-56}$
Layer 23	0.1346	0.0	-67.1515	0.0
Layer 24	0.1671	0.0	-5.2423	$1.5862 \times 10^{-7}$
Layer 25	0.1376	0.0	-2.9775	$2.9063 \times 10^{-3}$
Layer 26	0.1837	0.0	90.9769	0.0
Layer 27	0.1319	0.0	67.0804	0.0
Layer 28	0.1768	0.0	57.1779	0.0
Layer 29	0.0594	0.0	117.4058	0.0
Layer 30	0.0464	0.0	-25.2003	$3.9785 \times 10^{-140}$
Layer 31	0.1882	0.0	-53.1113	0.0

Table 7: FFN Activations Variance and Kurtosis Values per Layer for Lama 3

Layer	Aligned Variance	Misaligned Variance	Aligned Kurtosis	Misaligned Kurtosis
Layer 0	0.000212	0.000510	32.757828	364.158944
Layer 1	0.236660	0.236592	344029.010913	344226.518989
Layer 2	0.000295	0.000353	7.127898	45.979829
Layer 3	0.000518	0.000487	59.649299	4.726789
Layer 4	0.000692	0.000715	0.795759	0.362406
Layer 5	0.000950	0.001229	0.477034	0.852841
Layer 6	0.001250	0.001461	24.752695	29.889093
Layer 7	0.001621	0.001776	6.151176	18.224953
Layer 8	0.001597	0.001505	2.469859	3.624184
Layer 9	0.002246	0.001545	93.514968	38.368989
Layer 10	0.001963	0.001711	4.624561	4.741636
Layer 11	0.002067	0.001839	0.619448	8.063537
Layer 12	0.002094	0.001896	9.832133	7.831309
Layer 13	0.002460	0.001997	0.611578	0.918006
Layer 14	0.002863	0.002267	15.886125	1.421881
Layer 15	0.002851	0.002462	2.923889	4.253402
Layer 16	0.002688	0.002407	16.426754	10.997486
Layer 17	0.002636	0.002389	12.949386	40.475359
Layer 18	0.001896	0.001674	6.559782	12.719294
Layer 19	0.001825	0.001916	64.318771	64.902025
Layer 20	0.002072	0.001920	60.462527	39.985912
Layer 21	0.002854	0.002619	37.429808	90.184434
Layer 22	0.002032	0.001965	61.272983	98.871141
Layer 23	0.001838	0.001695	3.972599	9.586147
Layer 24	0.002926	0.002369	4.804575	3.953097
Layer 25	0.002487	0.002513	25.634998	28.264629
Layer 26	0.005470	0.005264	58.637025	36.473062
Layer 27	0.008895	0.008619	0.528337	2.938631
Layer 28	0.010616	0.011235	2.364869	3.982332
Layer 29	0.022143	0.022959	92.879826	93.424681
Layer 30	0.079033	0.084350	81.294238	83.782203
Layer 31	1.135274	1.216739	14399.446705	12585.702823

Table 8: Activations Entropy and Number of Peaks per Layer for Llama 3

Layer	Aligned Entropy	Misaligned Entropy	Aligned Peaks	Misaligned Peaks
Layer 0	1.390817	1.430737	41	127
Layer 1	0.000465	0.000495	49	108
Layer 2	2.313199	2.350038	41	112
Layer 3	2.148607	2.174024	40	125
Layer 4	2.772901	2.794252	43	80
Layer 5	2.632099	2.757681	42	122
Layer 6	2.189469	2.260520	42	112
Layer 7	2.401442	2.433842	42	123
Layer 8	2.352235	2.321993	43	92
Layer 9	1.741799	1.592606	43	107
Layer 10	2.172766	2.104282	43	90
Layer 11	2.958910	2.886623	42	65
Layer 12	2.359208	2.314337	40	77
Layer 13	2.683580	2.580417	41	127
Layer 14	2.200285	2.099395	39	90
Layer 15	2.474309	2.402266	42	85
Layer 16	2.297885	2.244245	37	122
Layer 17	2.198479	2.126024	40	85
Layer 18	1.678259	1.613673	38	116
Layer 19	2.149443	2.159631	40	126
Layer 20	2.183639	2.158820	33	126
Layer 21	2.071865	1.989183	39	118
Layer 22	2.120278	2.078059	43	126
Layer 23	2.316166	2.266680	33	127
Layer 24	2.709468	2.606097	41	127
Layer 25	2.244663	2.255491	40	113
Layer 26	2.247325	2.247983	40	122
Layer 27	3.000723	2.976391	31	104
Layer 28	2.694904	2.718854	32	126
Layer 29	2.196106	2.211723	41	106
Layer 30	2.064699	2.085282	28	103
Layer 31	0.059853	0.064633	40	125



Table 9: Means and Standard Deviations of Activations on Llama 3.1

Layer	Aligned Mean	Aligned Std	Misaligned Mean	Misaligned Std
Layer 0	0.0002	0.0201	0.0002	0.0285
Layer 1	-0.0003	0.6456	-0.0007	0.6529
Layer 2	0.0001	0.0213	-0.0000	0.0212
Layer 3	-0.0007	0.0280	-0.0000	0.0283
Layer 4	-0.0001	0.0320	-0.0002	0.0342
Layer 5	0.0003	0.0411	0.0001	0.0420
Layer 6	-0.0006	0.0474	0.0002	0.0447
Layer 7	-0.0006	0.0542	-0.0003	0.0517
Layer 8	-0.0009	0.0509	-0.0011	0.0491
Layer 9	-0.0003	0.0510	0.0001	0.0495
Layer 10	-0.0010	0.0567	0.0002	0.0531
Layer 11	-0.0006	0.0570	-0.0004	0.0556
Layer 12	0.0009	0.0601	0.0002	0.0565
Layer 13	-0.0015	0.0618	-0.0010	0.0574
Layer 14	-0.0000	0.0641	-0.0004	0.0626
Layer 15	-0.0002	0.0692	-0.0001	0.0644
Layer 16	-0.0009	0.0635	-0.0009	0.0623
Layer 17	-0.0001	0.0586	0.0004	0.0624
Layer 18	0.0005	0.0516	0.0002	0.0542
Layer 19	0.0001	0.0534	0.0005	0.0552
Layer 20	-0.0002	0.0545	-0.0002	0.0595
Layer 21	0.0004	0.0649	0.0002	0.0693
Layer 22	-0.0003	0.0534	-0.0003	0.0588
Layer 23	-0.0005	0.0519	-0.0004	0.0568
Layer 24	-0.0004	0.0643	0.0000	0.0662
Layer 25	-0.0022	0.0614	-0.0023	0.0668
Layer 26	0.0013	0.0946	0.0002	0.0993
Layer 27	-0.0020	0.1230	-0.0019	0.1287
Layer 28	-0.0010	0.1285	-0.0005	0.1408
Layer 29	0.0016	0.1895	0.0021	0.2162
Layer 30	0.0101	0.3671	0.0126	0.4100
Layer 31	0.0278	1.2928	0.0332	1.4824

Table 10: Statistical Tests Results on Llama 3.1 FFN activations

Layer	KS Statistic	KS p-value	t-Statistic	t p-value
Layer 0	0.0077	0	7.0726	$1.5203 \times 10^{-12}$
Layer 1	0.0338	0	5.0025	$5.6581 \times 10^{-07}$
Layer 2	0.0075	0	22.8735	$8.5424 \times 10^{-116}$
Layer 3	0.0138	0	-167.8477	0
Layer 4	0.0164	0	24.3150	$1.3607 \times 10^{-130}$
Layer 5	0.0039	0	35.4805	$9.8455 \times 10^{-276}$
Layer 6	0.0202	0	-119.8975	0
Layer 7	0.0166	0	-44.7754	0
Layer 8	0.0111	0	25.2201	$2.4134 \times 10^{-140}$
Layer 9	0.0092	0	-62.0720	0
Layer 10	0.0204	0	-152.6716	0
Layer 11	0.0130	0	-24.3901	$2.1775 \times 10^{-131}$
Layer 12	0.0211	0	94.5910	0
Layer 13	0.0227	0	-63.4716	0
Layer 14	0.0119	0	39.8030	0
Layer 15	0.0176	0	-15.0153	$5.8282 \times 10^{-51}$
Layer 16	0.0075	0	5.3294	$9.8537 \times 10^{-08}$
Layer 17	0.0083	0	-50.0778	0
Layer 18	0.0102	0	47.7368	0
Layer 19	0.0125	0	-48.6066	0
Layer 20	0.0179	0	-0.4807	$6.3075 \times 10^{-01}$
Layer 21	0.0146	0	21.3121	$8.7696 \times 10^{-101}$
Layer 22	0.0235	0	-2.5624	$1.0396 \times 10^{-02}$
Layer 23	0.0186	0	-6.4478	$1.1345 \times 10^{-10}$
Layer 24	0.0088	0	-44.2329	0
Layer 25	0.0199	0	16.1789	$7.1097 \times 10^{-59}$
Layer 26	0.0101	0	78.6355	0
Layer 27	0.0053	0	-3.0907	$1.9969 \times 10^{-03}$
Layer 28	0.0156	0	-29.7396	$2.3682 \times 10^{-194}$
Layer 29	0.0052	0	-20.5584	$6.4724 \times 10^{-94}$
Layer 30	0.0162	0	-47.5514	0
Layer 31	0.0173	0	-27.9946	$1.8894 \times 10^{-172}$

Table 11: FFN Activations Variance and Kurtosis Values per Layer for Lama 3.1

Layer	Aligned Variance	Misaligned Variance	Aligned Kurtosis	Misaligned Kurtosis
Layer 0	0.000404	0.000814	38.748624	375.936553
Layer 1	0.416794	0.426272	341318.653228	326343.909150
Layer 2	0.000453	0.000449	2.488627	12.863954
Layer 3	0.000787	0.000799	25.004033	1.678751
Layer 4	0.001022	0.001166	1.416729	0.632352
Layer 5	0.001692	0.001765	0.312195	1.244076
Layer 6	0.002248	0.001996	13.021483	11.426331
Layer 7	0.002943	0.002671	7.567117	11.564255
Layer 8	0.002586	0.002412	2.057977	1.248498
Layer 9	0.002596	0.002450	26.146935	15.778057
Layer 10	0.003216	0.002822	29.333605	12.334599
Layer 11	0.003248	0.003093	2.299698	6.174563
Layer 12	0.003606	0.003190	2.867246	9.256613
Layer 13	0.003824	0.003291	0.942112	1.653039
Layer 14	0.004103	0.003913	0.351336	2.828304
Layer 15	0.004794	0.004151	5.085419	5.363530
Layer 16	0.004036	0.003882	5.812460	8.859311
Layer 17	0.003435	0.003888	10.594112	32.042719
Layer 18	0.002664	0.002934	13.339556	16.267094
Layer 19	0.002851	0.003044	24.409184	31.016534
Layer 20	0.002967	0.003543	23.392221	26.467337
Layer 21	0.004215	0.004808	47.326836	69.573910
Layer 22	0.002855	0.003463	102.317790	102.110836
Layer 23	0.002698	0.003228	5.542072	37.362970
Layer 24	0.004130	0.004378	5.052662	4.294181
Layer 25	0.003768	0.004465	16.485577	51.648008
Layer 26	0.008952	0.009870	63.531770	66.936732
Layer 27	0.015138	0.016553	0.500493	10.788369
Layer 28	0.016514	0.019820	2.323452	14.297032
Layer 29	0.035926	0.046728	88.718032	234.520944
Layer 30	0.134786	0.168077	78.316231	157.494293
Layer 31	1.671414	2.197644	19658.055751	11466.254428

Table 12: Activations Entropy and Number of Peaks per Layer for Llama 3.1

Layer	Aligned Entropy	Misaligned Entropy	Aligned Peaks	Misaligned Peaks
Layer 0	1.422649	1.411817	36	127
Layer 1	0.000538	0.000923	41	96
Layer 2	2.478942	2.457450	41	71
Layer 3	2.324757	2.367522	40	111
Layer 4	2.771986	2.841603	41	106
Layer 5	2.763314	2.778450	45	102
Layer 6	2.380713	2.326703	33	97
Layer 7	2.513412	2.460572	40	115
Layer 8	2.313925	2.281893	36	77
Layer 9	1.822700	1.806551	42	99
Layer 10	1.956781	1.906546	41	99
Layer 11	2.812666	2.782584	39	96
Layer 12	2.452796	2.384898	41	80
Layer 13	2.487775	2.412252	34	120
Layer 14	2.716854	2.689150	34	122
Layer 15	2.424438	2.359523	43	86
Layer 16	2.352053	2.331200	39	122
Layer 17	2.015743	2.054148	38	111
Layer 18	1.514254	1.553786	40	89
Layer 19	2.108952	2.147636	39	117
Layer 20	2.479717	2.564007	34	126
Layer 21	1.880695	1.945309	37	107
Layer 22	1.953244	2.045247	34	115
Layer 23	2.146672	2.222197	35	122
Layer 24	2.639829	2.672478	40	114
Layer 25	2.309509	2.395691	39	111
Layer 26	2.166277	2.218198	31	118
Layer 27	3.047661	3.071268	25	100
Layer 28	2.695442	2.768950	33	122
Layer 29	2.344540	2.395680	29	85
Layer 30	2.105706	2.178419	31	117
Layer 31	0.064270	0.086658	28	119